The following publication J. M. Liang et al., "Observation of Interfacial Antiferromagnetic Coupling Between Ferrimagnetic Garnet Thin Films," in IEEE Transactions on Magnetics, vol. 58, no. 2, pp. 1-5, Feb. 2022, Art no. 2200205 is available at https://doi.org/10.1109/TMAG.2021.3087822

Observation of Interfacial Antiferromagnetic Coupling between Ferrimagnetic Garnet Thin Films

Jing Ming Liang[1], Xu Wen Zhao[1], Sheung Mei Ng[1], Hon Fai Wong[1], Yu Kuai Liu[1,2], Chee Leung Mak[1], and Chi Wah Leung*[1]

[1]Department of Applied Physics, The Hong Kong Polytechnic University, Hung Hom, Hong Kong, China
[2]College of Electronic Information and Mechatronic Engineering, Zhaoqing University, Zhaoqing 526061, Guangdong, China

We report a study on the interfacial antiferromagnetic coupling between ferrimagnetic TbIG/YIG thin films. TbIG/YIG bilayer films are grown on YAG (110) substrates. The crystal structure and magnetic properties of the films are characterized. The temperature and directional dependences of the antiferromagnetic coupling effect are observed at low temperatures. This work enriches the magnetic research of ferrimagnetic oxide films with complex structures, providing new ideas for the design of antiferromagnetically coupled spintronics devices.

***Index Terms*—Antiferromagnetic coupling, Inverted hysteresis loop, YIG, TbIG**

I. Introduction

Antiferromagnetic coupling among magnetic layers has long been investigated since its observation in Fe/Cr multilayers [1], and plays a significant role in the development of spintronic devices [2]. For example, Song *et al*. fabricated MgO/CoFeB/Ta/CoFeB/MgO multilayers, which allow magnetic memories with low stray fields due to the antiferromagnetic coupling between the CoFeB layers [3]. While such coupling has been widely reported in metallic multilayers, it is seldom reported in the more complex magnetic oxide multilayer films [4-6].

Yttrium iron garnet ($Y_3Fe_5O_{12}$, YIG) is a ferrimagnetic oxide with antiferromagnetic coupling between Y and Fe sublattices [7], and has recently attracted interest due to the possibility of converting magnon excitations into spin and charge signals [8,9]. Iron garnets with Y substituted by other rare-earth ions exist (such as $Tb_3Fe_5O_{12}$, TbIG), and the different temperature dependences of the rare-earth and Fe ions leads to a compensation temperature (T_{comp}) at which the net magnetization momentarily vanishes [10]. The phenomenon of magnetization compensation is of interest for spintronics applications [11]. For example, with the absence of internal dipole fields, it is conducive to the formation of multi-stable antiferromagnetic domains, and this can be used in magnetic tunnel junctions with logic functions [12].

Here we study the antiferromagnetic coupling at the interface of epitaxial TbIG/YIG bilayers grown on $Y_3Al_5O_{12}$ (YAG) substrates, being manifested in form of inverted hysteresis loop at low temperatures. Such antiferromagnetic coupling has been previously reported in bilayers of YIG/$Gd_3Fe_5O_{12}$ (GdIG), as inferred from spin-Hall magnetoresistance measurements [4]. The effect exhibits a strong temperature dependence, and directional dependence of such coupling is also observed. A simple model based on the coupling between Tb- and Fe-ions across the bilayer interface is used to explain the observations.

II. Experiments

Epitaxial TbIG (30 nm), YIG (30 nm), and TbIG (7 nm)/YIG (23 nm) (from the bottom to the top) films were deposited on YAG (110) single crystal substrates by pulsed laser deposition (PLD), in a chamber with base pressure better than 2×10^{-6} mTorr. Before film deposition, the substrates were rinsed with acetone, alcohol, and deionized water, and then annealed in air at 1000°C for 6 h. These steps promote the surface reconstruction of the substrates, which is conducive to smooth film growth [13]. The films were deposited in 100 mTorr oxygen at 983 K, by a 248 nm KrF excimer laser with a pulse energy of 220 mJ and a repetition rate of 2 Hz. *In situ* post-annealing was performed at film deposition temperature for 10 min in 10 Torr oxygen ambient and subsequently cooled down naturally to room temperature. A control sample with 5 nm $Gd_3Ga_5O_{12}$ (GGG) spacer between TbIG and YIG was also prepared under identical conditions.

The microstructure of the samples was determined by high-resolution X-ray diffractometer (XRD, Rigaku Smartlab). Surface morphology of samples was characterized by atomic force microscopy (AFM, Asylum 3D infinity). Magnetic properties of the samples were measured by the vibrating sample magnetometer (VSM) option of the physical property measurement system (PPMS, Quantum Design), with the magnetic field applied along two perpendicular in-plane directions ([111] and $[11\bar{2}]$). Unless otherwise specified, the magnetic field directions in the following VSM tests were along with the $[11\bar{2}]$ direction in the film plane.

III. Results and Discussion

Fig. 1 (a) shows the $\theta/2\theta$ scans of YIG (30 nm), TbIG (30 nm), and TbIG (7 nm)/YIG (23 nm) bilayer films. Alongside the sharp (220) peak from the YAG substrate, (220) peaks of the films can be identified and no impurity peak is observed. From the figure, the lattice spacing d_{220} for YIG (4.395 Å) and TbIG (4.439 Å) is extracted, both of which are larger than the

corresponding bulk values (4.374 Å and 4.396 Å for YIG and TbIG, respectively), which can be attributed to the compressive in-plane stress from the YAG substrate (4.247 Å). Because of the similar lattice constants between YIG (12.376 Å) and TbIG (12.460 Å) and the small thickness of the TbIG layer, only a single (220) peak emerges in the TbIG/YIG bilayer [14], with the nominal d_{220} spacing (4.404 Å) in between that of YIG and TbIG single layers. Extensive interdiffusion between the layers is unlikely, based on our previous study of TbIG/GGG bilayers [15].

Fig. 1(b) presents the rocking curve of the (220) peak in the TbIG/YIG bilayer, the full-width at half-maximum (FWHM) of which is about 0.064° (as in contrast to 0.071° and 0.068° for YIG and TbIG single layers, respectively), indicating highly textured growth with low mosaic spread. AFM scan of the bilayer surface (inset, Fig. 1(b)) shows terrace-featured topography with a small root-mean-square roughness of 0.38 nm, signifying the good quality of the films.

Fig. 1(c) and (d) show the in-plane magnetic hysteresis (M-H) loops of YIG (30 nm) and TbIG (30 nm) films at 10 K (with the linear diamagnetic background of YAG substrate subtracted). While YIG has a small coercivity ($H_{c\text{-}YIG} \approx 190$ Oe, inset of Fig. 1(c)), TbIG exhibits a higher coercivity ($H_{c\text{-}TbIG} \approx$ 5.5 kOe) due to the strong magnetocrystalline anisotropy [16]. The strong contribution from the Tb^{3+} also leads to a higher saturation magnetization (M_s) of TbIG ($\approx$ 290 emu/cm^3) than YIG ($\approx$ 90 emu/cm^3) at low temperatures.

Fig. 2 demonstrates the M-H loops of the multilayered samples at 10 K. An obvious double coercivity phenomenon due to the drastically different H_c of the two layers can also be observed from the M-H loops. The switching at the low field is attributed to YIG, while the reversal at the high field is due to the reversal of TbIG: because of the high coercivity in TbIG, it requires a larger field to complete magnetization reversal, while the soft YIG layer can be reversed with a moderate field.

The most outstanding feature of the M-H loop in Fig. 2(a) is the inversion of the forward and backward traces in the low field region (inset, Fig. 2(a)): when the external field decreases from positive saturation, the YIG magnetization first reverses at a small *positive* field, while the magnetization of TbIG remains undisturbed. This clearly indicates the antiferromagnetic coupling between the TbIG/YIG at the interface [17-19]. To verify the effect is due to the interfacial coupling between the layers, a control sample with a 5 nm GGG spacer between TbIG and YIG was also measured (Fig. 2(b)). With the GGG spacer inserted, the interfacial coupling between TbIG and YIG is clearly suppressed, and one only observes a typical double-coercivity M-H loop while the inverted loop at low field disappears. This indicates the inverted loop at the low field is caused by the interfacial coupling of two garnet layers.

Fig. 3 (a) shows the temperature dependence of in-plane M-H loops for the TbIG (7 nm)/YIG (23 nm) sample. As temperature decreases, the M_s gradually increases and the double coercivity behavior becomes more pronounced. This is due to the stronger temperature dependence of the TbIG magnetization compared YIG [20] (see also Supplementary Information). Fig. 3 (b) is the enlarged view of the low-field region of Fig. 3 (a). Notice that the M-H loops change from normal to inverted state when the temperature is below 40 K, and such an effect becomes more pronounced at lower temperatures. The inverted hysteresis loop can be considered as a sign of antiferromagnetic coupling between two magnetic materials [21,22]. The strength of the coupling should depend on the interfacial magnetizations of the TbIG and YIG layers. Given the strong temperature dependence of the TbIG magnetization (dropping by half as temperature rises from 10 K to 50 K, see Supplementary Information), the effect is quickly overcome by other energy terms (such as Zeeman term of the YIG layer) and hence the invert loop behavior disappears even at 40 K [10].

Both YIG and TbIG belong to the cubic centrosymmetric space group *Ia3d* [20,21], with the primitive unit cell containing 80 atoms. Two 1/8 unit cells corresponding to YIG and TbIG at the interface are shown in Fig. 4. (a). The magnetic structure as determined by neutron diffraction measurements [23] suggests that the spins of the *A*-site Fe^{3+} and *D*-site Fe^{3+} are locked into an anti-parallel configuration, and the magnetization ratio is 2:3 for the *A*- and *D*-sites Fe^{3+} in the unit cell. Therefore, in YIG the net magnetic moment is determined by *D*-site Fe^{3+} as the *C*-site Y^{3+} is not magnetic. However, in TbIG, since the magnetic moment of *C*-site Tb^{3+} is weakly coupled with *A*-sites Fe^{3+}, the net magnetic moment of TbIG is determined by the coupling effect between the *C*- and *D*-site ions, and this *C*-*D* coupling is strongly temperature-dependent [24]. At high temperatures, the magnetization of TbIG is determined by the *D*-site Fe^{3+}. With decreasing temperature, the magnetization of the Tb^{3+} strongly increases, and together with the *A*-site Fe^{3+} magnetization eventually overcomes the anti-paralleled *D*-site Fe^{3+} magnetization.

We argue that the interfacial antiferromagnetic coupling arises from the interaction between Tb^{3+} in TbIG and Fe^{3+} in YIG. As shown in Fig. 4 (b), when a strong external magnetic field (H) is applied in-plane, the net magnetic moment in YIG and TbIG are aligned with H. When H is gradually reduced to 0, the rotation of Fe^{3+} moment in the YIG layer appears first, while the magnetic moment of Tb^{3+} remain unchanged due to its larger coercivity. At this time, the antiferromagnetic coupling between *C*-site Tb^{3+} of TbIG and *D*-sites Fe^{3+} of YIG at the TbIG/YIG interface forces the reversal of the YIG magnetization (Fig. 4 (c)), leading to the inverted M-H loop (Fig. 2 (a)). When H increases to saturation state in the opposite direction (Fig. 4(d)), the magnetic moment of Tb^{3+} completes its reversal, and the arrangement of the magnetic moments is the same as in Fig. 4 (b) but in the opposite direction.

We note with caution that the above explanation has not taken in account the complicated magnetization structure in TbIG bulk at various temperatures (e.g. the "double-umbrella" structure of the Tb^{3+} ions below around 160 K [25,26]), and there is even less detailed investigation of magnetization in ultrathin garnet thin films. However, the simple model

apparently has captured the essence of the coupling behaviour and is subjected to refinement with further experimentations.

For films grown on (110) substrates, magnetic anisotropy variations are expected along with perpendicular in-plane directions [27]. We, therefore, measured the M-H loops of the TbIG (7 nm)/YIG (23 nm) bilayer at 10 K along with the two perpendicular directions of [111] and $[11\bar{2}]$. It is worth noting that while TbIG/YIG exhibit in-plane anisotropy, the antiferromagnetic coupling effect between the two garnet films depends on the direction: measurement along with external $[11\bar{2}]$ shows an obvious inverted hysteresis loop (Inset A), but a normal M-H loop is obtained when it is measured in the [111] direction (Inset B). Preliminary magnetization measurements of TbIG (7 nm)/YIG (23 nm) deposited on YAG(111) also demonstrated inverted loop behaviour (Supplementary Information), which will be subjected to further studies.

Many reports have demonstrated in-plane uniaxial anisotropy in epitaxial YIG thin films grown on YAG or GGG single crystal substrates [22,28], which will lead to angle-dependent M-H loops when in-plane *H* is applied in different directions. The results in Fig. 5 suggest that the antiferromagnetic coupling between TbIG and YIG thin films is also affected by the presence of uniaxial anisotropy [29-31]. The origin of such an effect needs further investigation.

IV. Conclusions

In summary, interfacial antiferromagnetic coupling effect has been observed between two neighboring ferrimagnets films YIG and TbIG grown on the (110)-oriented YAG substrate, manifested in the form of an inverted hysteresis loop at a small magnetic field in low temperature. This phenomenon is postulated to be caused by the antiferromagnetic coupling between the *C*-site Tb^{3+} of TbIG and the *D*-site Fe^{3+} in YIG. The temperature-dependence of such an antiferromagnetic coupling effect of samples has been studied, which is due to the gradual dominance of Tb^{3+} magnetism as the temperature decreases. Moreover, this antiferromagnetic coupling effect shows preference in orientation. The present work should be useful for the further development of ferrimagnetic insulator-based spintronics.

Acknowledgment

Financial support by the RGC, HKSAR (PolyU 15302320) is acknowledged.

References

[1] P. Grunberg, R. Schreiber, Y. Pang, M. B. Brodsky, and H. Sowers, "Layered magnetic structures: Evidence for antiferromagnetic coupling of Fe layers across Cr interlayers," *Physical Review Letters*, vol. 57, no. 19, pp. 2442-2445, 1986.

[2] R. A. Duine, K. J. Lee, S. S. P. Parkin, and M. D. Stiles, "Synthetic Antiferromagnetic Spintronics," *Nature Physics*, vol. 14, no. 3, pp. 217-219, 2018.

[3] G. Y. Shi et al., "Spin-orbit torque in MgO/CoFeB/Ta/CoFeB/MgO symmetric structure with interlayer antiferromagnetic coupling," *Physical Review B*, vol. 95, no. 10, 2017.

[4] J.M. Gomez-Perez et al., "Synthetic Antiferromagnetic Coupling Between Ultrathin Insulating Garnets", *Phys. Rev. Appl.* vol. 10, no. 4, 044046, 2018.

[5] G. Avvisati et al., "Ferromagnetic and Antiferromagnetic Coupling of Spin Molecular Interfaces with High Thermal Stability," *Nano Letters*, vol. 18, no. 4, pp. 2268-2273, 2018.

[6] T. Maity, D. Kepaptsoglou, M. Schmidt, Q. Ramasse, and S. Roy, "Observation of complete inversion of the hysteresis loop in a bimodal magnetic thin film," *Physical Review B*, vol. 95, no. 10, 2017.

[7] L. S. Xie et al., "First-principles study of exchange interactions of yttrium iron garnet," *Physical Review B*, vol. 95, no. 1, 2017.

[8] H. Nakayama et al., "Spin Hall magnetoresistance induced by a nonequilibrium proximity effect," *Physical Review Letters*, vol. 110, no. 20, p. 206601, 2013.

[9] L. Wang et al., "Electrical Control of Spin-Mixing Conductance in a $Y_3Fe_5O_{12}$/Platinum Bilayer," *Physical Review Applied*, vol. 11, no. 4, p. 044060, 2019.

[10] S. Geller, J. P. Remeika, R. C. Sherwood, H. J. Williams, and G. P. Espinosa, "Magnetic Study of the Heavier Rare-Earth Iron Garnets," *Physical Review*, vol. 137, no. 3A, pp. A1034-A1038, 1965.

[11] J. Železný, P. Wadley, K. Olejník, A. Hoffmann, and H. Ohno, "Spin transport and spin torque in antiferromagnetic devices," *Nature Physics*, vol. 14, no. 3, pp. 220-228, 2018.

[12] A. Niemeyer, G. Reiss, and H. Brückl, "Magnetic tunnel junctions with compensated magnetic moment by directly exchange-coupled NiFe/CoGd/NiFe trilayers," *Applied Physics Letters*, vol. 88, no. 18, p. 182503, 2006.

[13] Y. K. Liu, et al., "Anomalous Hall effect in Pt/$Tb_3Fe_5O_{12}$ heterostructure: Effect of compensation point," *Journal of Magnetism and Magnetic Materials*, vol. 468, pp. 235-240, 2018.

[14] S. Mokarian Zanjani and M. C. Onbaşlı, "Predicting new iron garnet thin films with perpendicular magnetic anisotropy," *Journal of Magnetism and Magnetic Materials*, vol. 499, p. 166108, 2020.

[15] Y.K. Liu et al., "Strain dependent structure and anomalous Hall effect in Pt/$Tb_3Fe_5O_{12}$/$Ga_3Gd_5O_{12}$ heterostructure grown on $Y_3Al_5O_{12}$ substrates". *J. Magn. Magn. Mater*., DOI: 10.1016/j.jmmm.2021.168130 (2021).

[16] R. F. Pearson, "Magnetocrystalline Anisotropy of Rare-Earth Iron Garnets," *Journal of Applied Physics*, vol. 33, no. 3, pp. 1236-1242, 1962.

[17] H. Zhang et al., "Antiferromagnetic interlayer coupling of (111)-oriented $La_{0.67}Sr_{0.33}MnO_3$/$SrRuO_3$ superlattices," *Chinese Physics B*, vol. 28, no. 3, pp. 037501, 2019.

[18] T. Maity, D. Kepaptsoglou, M. Schmidt, Q. Ramasse, and S. Roy, "Observation of complete inversion of the hysteresis loop in a bimodal magnetic thin film." *Physical Review B*, vol. 95, no. 10, p. 100401, 2017.

[19] M. Saghayezhian et al., "Atomic-scale determination of spontaneous magnetic reversal in oxide heterostructures," *Proceedings of the National Academy of Sciences*, vol. 116, no. 21, pp. 10309-10316, 2019.

[20] M. Uemura, T. Yamagishi, S. Ebisu, S. Chikazawa, and S. Nagata, "A double peak of the coercive force near the compensation temperature in the rare earth iron garnets," *Philosophical Magazine*, vol. 88, no. 2, pp. 209-228, 2008.

[21] M. Saghayezhian et al., "Exchange bias and inverted hysteresis in monolithic oxide films by structural gradient," *Physical Review Research*, vol. 1, no. 3, pp. 033160, 2019.

[22] P. Liu and J. K. Tang, "A magnetic polaron model for the enhanced Curie temperature of EuO_{1-x},", *Journal of Physics: Condensed Matter*, vol. 25, no. 12, p. 125802, 2013.

[23] L. S. Xie et al., "First-principles study of exchange interactions of yttrium iron garnet." *Physical Review B*, vol. 95, no. 1, p. 014423, 2017.

[24] K. P. Belov, "Ferrimagnets with a 'weak' magnetic sublattice," *Physics-Uspekhi*, vol. 39, no. 6, pp. 623-634, 1996.

[25] Lahoubi, M. (2012). Temperature evolution of the double umbrella magnetic structure in terbium iron garnet. Neutron Diffraction, 203-230.

[26] Lahoubi, M., Guillot, M., Marchand, A., Tcheou, F., & Roudault, E. (1984). Double umbrella structure in terbium iron garnet. IEEE Transactions on Magnetics, 20(5), 1518-1520.

[27] L. M. Berndt, V. Balbarin, and Y. Suzuki, "Magnetic anisotropy and strain states of (001) and (110) colossal magnetoresistance thin films," *Applied Physics Letters*, vol. 77, no. 18, pp. 2903-2905, 2000.

[28] C. Vittoria, H. Lessoff, and N. Wilsey, "Induced in-plane magnetic anisotropy in YIG films," *IEEE Transactions on Magnetics*, vol. 8, no. 3, pp. 273-275, 1972.
[29] C. Tang et al., "Exquisite growth control and magnetic properties of yttrium iron garnet thin films," *Applied Physics Letters*, vol. 108, no. 10, pp. 102403, 2016.
[30] B. B. Krichevtsov et al., "Magnetization reversal in YIG/GGG(111) nanoheterostructures grown by laser molecular beam epitaxy," *Science and Technology of Advanced Materials*, vol. 18, no. 1, pp. 351-363, 2017.
[31] J. Mendil et al., "Magnetic properties and domain structure of ultrathin yttrium iron garnet/Pt bilayers," *Physical Review Materials*, vol. 3, no. 3, pp. 034403, 2019.

Figures

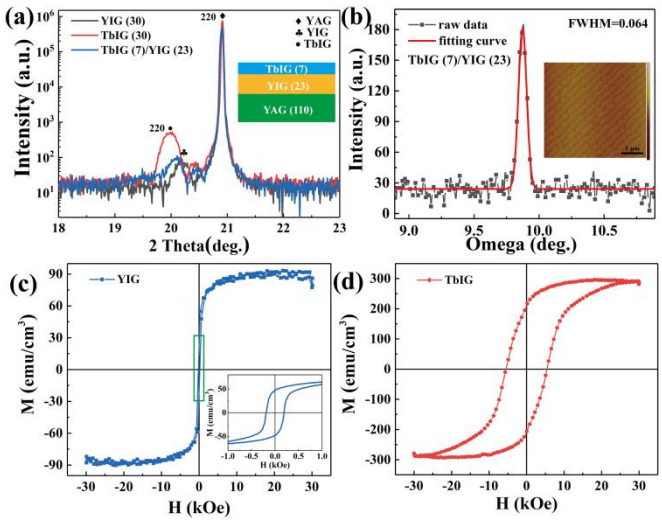

Fig. 1 (a) $\theta/2\theta$ of YIG (30 nm), TbIG (30 nm) single layers, and TbIG (7 nm)/YIG (23 nm) bilayer; schematic of the bilayer is shown in the inset. (b) The rocking curve of the bilayer sample, with the corresponding AFM image (scan height = 10 nm) shown in the inset. In-plane M-H loops of YIG (30 nm) and TbIG (30 nm) at 10 K are shown in (c) and (d), respectively. The inset of (c) is an enlarged view of the low-field region.

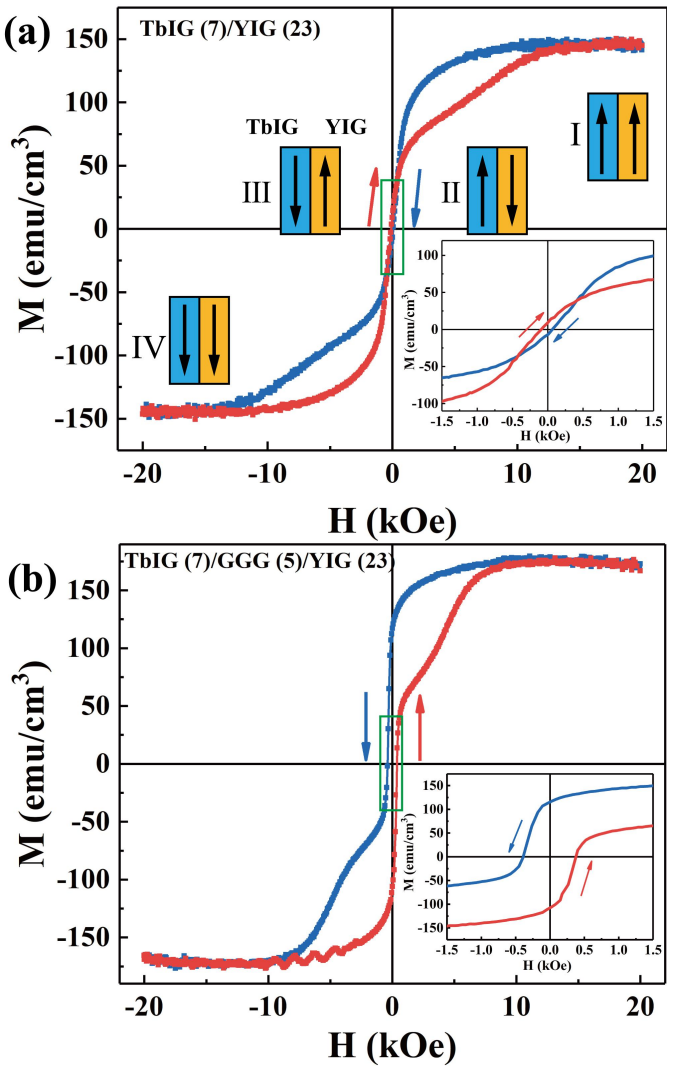

Fig. 2 In-plane M-H loops of TbIG (7 nm)/YIG (23 nm) (a) and TbIG (7 nm)/GGG (5 nm)/YIG (23 nm) (b) at 10 K. Insets show the enlarged signals at low fields. The relative magnetic orientation of TbIG and YIG is illustrated in the inset diagrams of Fig. 2(a). Arrows indicate the sweeping directions of the external magnetic field.

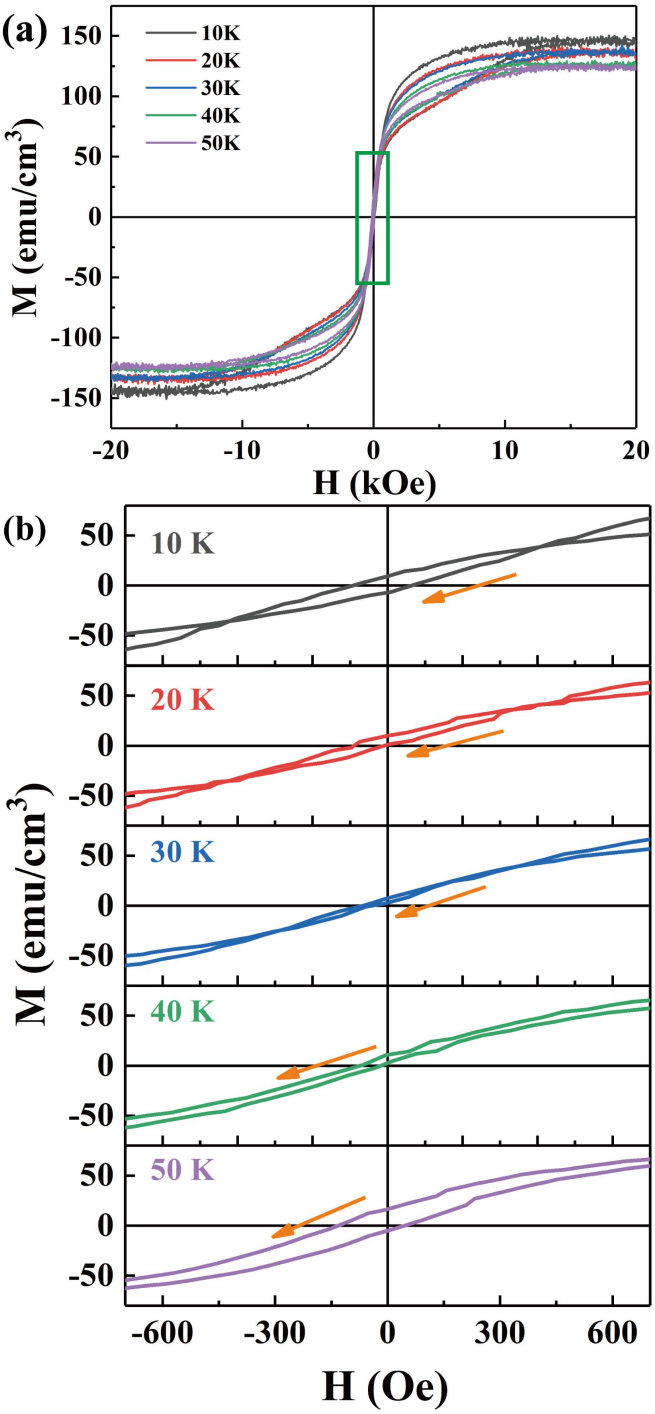

Fig. 3 Temperature dependence of interfacial coupling. (a) shows the in-plane M-H loops of TbIG (7 nm)/YIG (23 nm) sample at various temperatures, and (b) highlights the M-H loops at low fields. The arrows indicate the sweeping field directions.

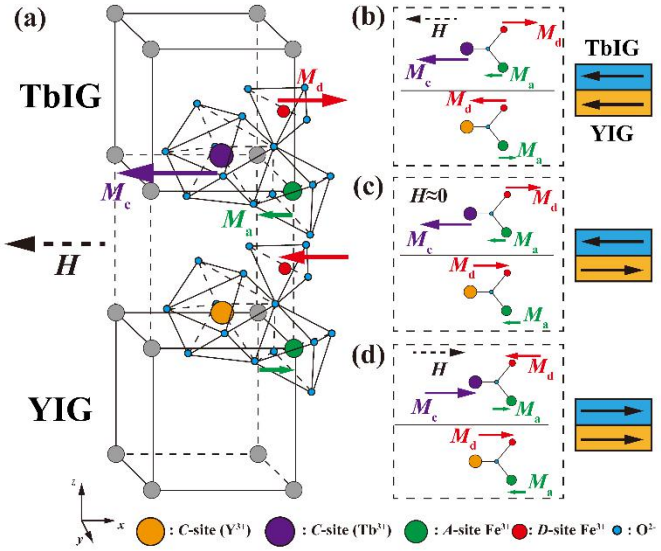

Fig. 4 (a) Skeleton drawing of two 1/8 of unit cells corresponding to YIG and TbIG at the interface. The unit cells have a garnet-type structure $(C)_3[A]_2(D)_3O_{12}$ with dodecahedral (*C*-site: Y^{3+} (yellow) or Tb^{3+} (purple)), octahedral [*A*-site: Fe^{3+} (green)], and tetrahedral (*D*-site: Fe^{3+} (red)) sites. The oxygen sites (blue) are for reference only, while all cation sites are in special crystallographic positions. *H* represents the direction of the external magnetic field. Fig. 4 (b) - (d) are schematic models of the evolution of the antiferromagnetic coupling effect between YIG and TbIG layers. M_c, M_a, and M_d represent the magnetic moment direction of *C*-site Tb^{3+}, *A*-site Fe^{3+}, and *D*-site Fe^{3+} ions, respectively

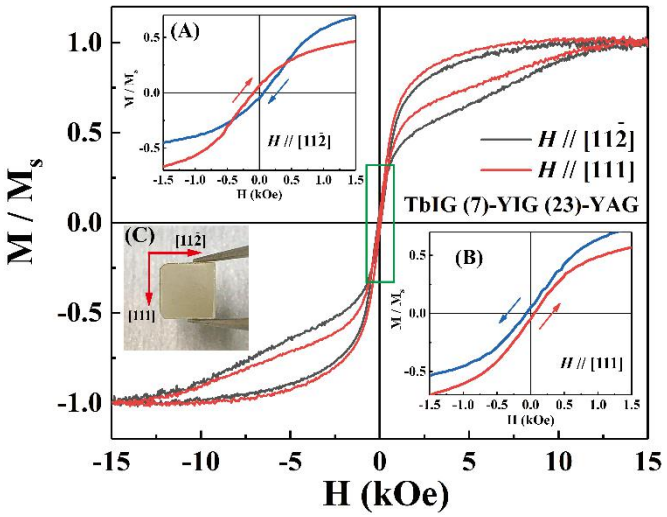

Fig. 5 In-plane M-H loops of TbIG (7 nm)/YIG (23 nm) sample at 10 K with external magnetic field along [11$\bar{2}$] and [111] directions. Insets (A) and (B) are the corresponding enlarged M-H loops at low field range with external magnetic field along [11$\bar{2}$] and [111] directions, respectively. The inset (C) is the actual photo of the sample, the two cut corners in the [111] direction are caused when cutting the YAG (110) substrate.